

# Probabilistic tsunami hazard assessment along Oman coast from submarine earthquakes in the Makran subduction zone

Issa El-Hussain<sup>1</sup> · Rachid Omira<sup>2</sup> · Ahmed Deif<sup>1,3</sup> · Zaid Al-Habsi<sup>1</sup> · Ghazi Al-Rawas<sup>1</sup> · Adel Mohamad<sup>1,3</sup> · Khalifa Al-Jabri<sup>1</sup> · Maria Ana Baptista<sup>4</sup>

Received: 23 May 2016 / Accepted: 19 September 2016 / Published online: 8 October 2016  
© Saudi Society for Geosciences 2016

**Abstract** The Sultanate of Oman is among the Indian Ocean countries that were subjected to at least two confirmed tsunamis during the twentieth and twenty-first centuries: the 1945 tsunami due to an earthquake in the Makran subduction zone in the Sea of Oman (near-regional field tsunami) and the Indian Ocean tsunami in 2004, caused by an earthquake from the Andaman Sumatra subduction zone (far - field tsunami). In this paper, we present a probabilistic tsunami hazard assessment for the entire coast of Oman from tectonic sources generated along the Makran subduction zone. The tsunami hazard is assessed taking into account the contribution of small- and large-event magnitudes. Results of the earthquake recurrence rate studies and the tsunami numerical modeling for different magnitudes were used through a logic-tree to estimate the tsunami hazard probabilities. We derive probability hazard exceedance maps for the Omani coast considering the exposure times of 100, 250, 500, and 1000 years. The hazard maps consist of computing the likelihood that tsunami waves exceed a specific amplitude. We find that the probability that a maximum wave amplitude exceeds 1 m somewhere along the coast of Oman reaches, respectively, 0.7 and 0.85 for 100 and 250 exposure times,

and it is up to 1 for 500 and 1000 years of exposure times. These probability values decrease significantly toward the southern coast of Oman where the tsunami impact, from the earthquakes generated at Makran subduction zone, is low.

**Keywords** Tsunami · Oman · Makran subduction zone · Probabilistic analysis

## Introduction

Natural disasters are the consequence of the impact of a natural hazard on a socioeconomic system with a given level of vulnerability. It is considered to be one of the most complex challenges facing human well-being, as well as sustainable development, all around the world. Tsunami, among all natural disasters, is one of the most dangerous natural hazards responsible for significant loss of life and property throughout history.

In the twentieth and twenty-first centuries, two tsunamis of tectonic origin impacted the coast of the Sultanate of Oman: the 1945 tsunami due to an earthquake in the Makran subduction zone (MSZ) in the Sea of Oman (near-field tsunami) and the Indian Ocean tsunami in 2004, due to an earthquake from Andaman Sumatra subduction zone (far - field tsunami).

The impact of the 1945 tsunami was large (Muscat Intelligence Summary 1945; Pendsee 1946; Heidarzadeh et al. 2007). It affected Pakistan, the western coast of India, Iran, and Oman, killing hundreds of people and causing significant destruction. Pendsee (1946) reports tsunami observations of 13 to 15 m in Pakistan. In Oman, the historical documents describe tsunami observations in Muscat and Sur with some damage, but no details are given. The impact of the Indian Ocean 2004 Sumatra tsunami was negligible along the northern coast affecting mainly the southern coast of Oman (Okal et al. 2006). The tsunami

✉ Issa El-Hussain  
elhussain@squ.edu.om

<sup>1</sup> Earthquake Monitoring Center, Sultan Qaboos University, P. O. Box 50, PC 123 Al-Khoudh, Muscat, Oman

<sup>2</sup> Instituto Português do Mar e da Atmosfera, Rua C do Aeroporto, 1749-077 Lisbon, Portugal

<sup>3</sup> National Research Institute of Astronomy and Geophysics (NRIAG), Helwan, Cairo, Egypt

<sup>4</sup> Instituto Superior de Engenharia de Lisboa, Instituto Politécnico de Lisboa, R. Conselheiro Emídio Navarro, 1, 1959-007 Lisbon, Portugal

reached Salalah tide station at 08:12 UTC with a maximum amplitude of the third wave of 1.65 m (Nagarajan et al. 2006; Rabinovich and Thomson 2007).

Oman is among the Indian Ocean countries exposed to high tsunami threat. The tsunami vulnerability of Oman increases due to the built of many critical infrastructures along the coast. Also, the urban concentration close to the sea and the need of direct access to the sea and maritime transportation increase tsunami exposure and vulnerability. Therefore, assessing tsunami hazard along the entire coast of Oman remains of great importance.

Tsunami hazard methods include the scenario-based (-deterministic approach) and the probabilistic approach. The deterministic approach uses specific scenarios and quite often considers the maximum credible scenario and computes the ensuing tsunami impact in the areas of interest. Probabilistic tsunami hazard assessment (PTHA) calculates the likelihood of tsunami impact using a large number of possible tsunami sources and including the contribution of small and large events (Geist and Parsons 2006; Power et al. 2007; González et al. 2009; Sørensen et al. 2012). PTHA can be performed for any tsunami hazard metrics (wave height, inundation depth, current speed, etc.) involving the derivation of probability exceedance maps (Geist and Lynett 2014). PTHA was firstly introduced by Rikitake and Aida (1988) to estimate the tsunami hazard along the Japanese coast, and more recently, a comprehensive probabilistic framework was presented by Geist and Parsons (2006). The logic-tree framework, first considered for probabilistic seismic hazard analysis (Coppersmith and Youngs 1986) and recently was adapted to assess the probabilistic tsunami hazard (Annaka et al. 2007; Burbidge et al. 2008; Lorito et al. 2015; Omira et al. 2016a), is recognized as a comprehensive method for PTHA. PTHA has a diverse range of applications such as insurance activity, land use planning, and prioritizing of mitigation measures.

In the Indian Ocean, several authors published studies on PTHA, namely, Burbidge et al. (2009), Heidarzadeh and Kijko (2011), Yadav et al. (2013), Hoechner et al. (2016), and Roshan et al. (2016). Some of these studies (Heidarzadeh and Kijko 2011; Hoechner et al. 2016) have partially addressed the tsunami hazard along the coast of Oman.

In this study, we present PTHA along the entire coast of Oman for tsunamis of tectonic origin generated in the MSZ. To do this, we developed a logic-tree framework that incorporates (i) definition of the tsunamigenic source zones within the MSZ; (ii) generation of the earthquake scenario database within each source zone (individual magnitudes and fault parameters); (iii) deriving the earthquake recurrence rate; (iv) numerical simulation of the tsunami, associated to each defined scenario, from the source to the target coast; and (v) deriving the tsunami probability of exceedance using statistical methods. We present the results of this study in terms of maps

expressing the probability of exceeding the threshold of 1 m wave amplitude for the exposure times of 100, 250, 500, and 1000 years. The threshold of 1 m wave height is selected in this work on the basis of the study by Allen and Greenslade (2010) that associates a land threat (major land inundation of low lying coastal areas, dangerous waves and strong ocean currents) to tsunami waves of amplitude exceeding 0.55 m.

### Geodynamic context and seismicity of the Makran subduction zone

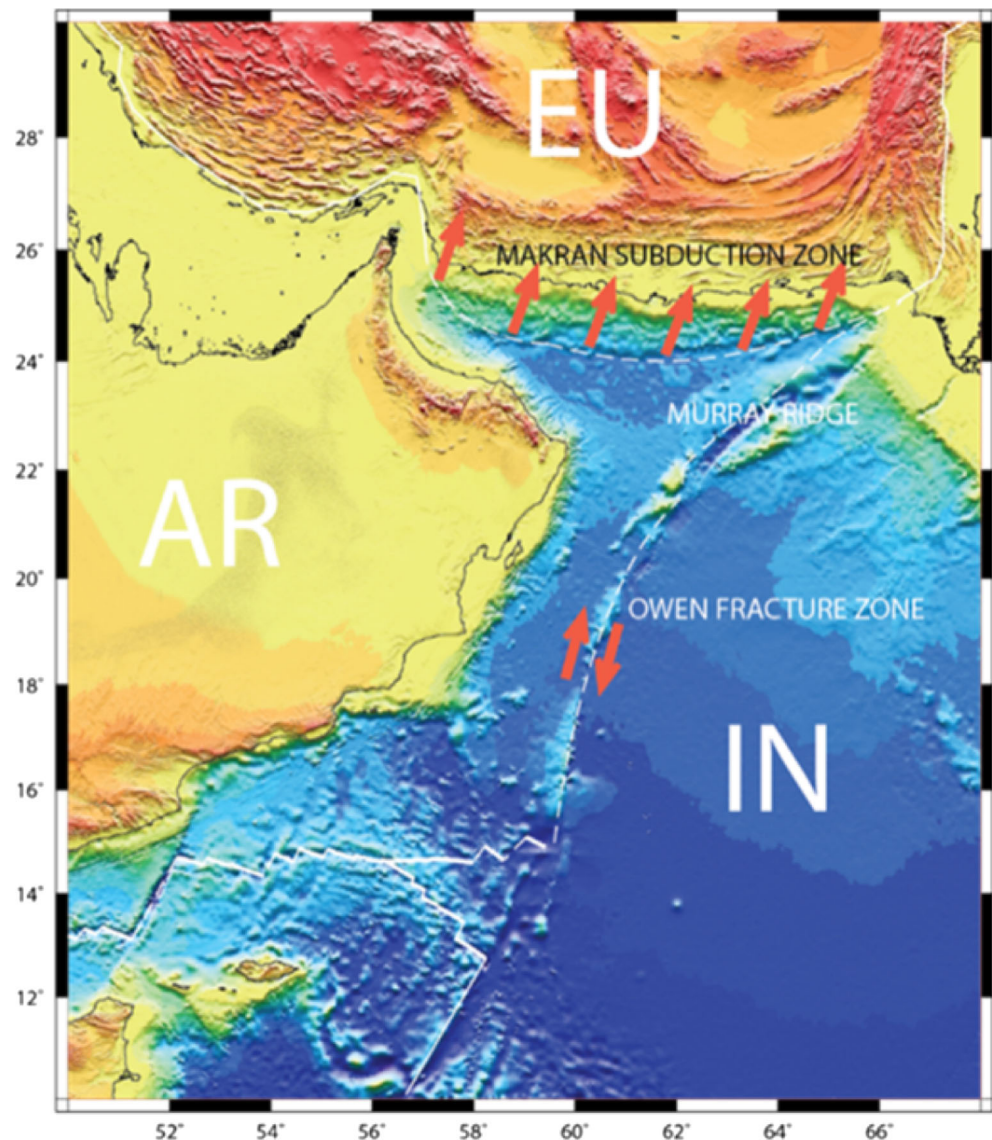
Oman occupies the southeastern part of the Arabian plate (Fig. 1), which is bordered by relatively active tectonic zones. For countries located in the northwest Indian Ocean, as it is the case of Oman, tsunami hazard is dominated by the seismic activity along the MSZ (Burbidge et al. 2009). MSZ stretches east from Iran to central Pakistan with a length of about 900 km. It is outcropped along a nearly E–W line under the Sea of Oman and the Arabian Sea, where their oceanic crust is subducting underneath the Eurasian plate since early Tertiary (Berberian and King, 1981; Harms et al. 1984; Kopp et al. 2000).

Two other major geological structures (Owen fracture zone and Murray ridge) are strike slip faults (Edwards et al. 2000; Fournier et al. 2011) and comparatively less active, as can be seen by the level of seismicity and the differential motion expected from global geodetic models (Wiens et al. 1985; DeMets et al. 2010; Rodriguez et al. 2013; Swapna and Srivastava 2014). Therefore, their tsunamigenic potential is much smaller compared to the Makran subduction zone and these are not included in this study. The Andaman Sumatra subduction zone constitutes the main far field tsunamigenic source as was clearly demonstrated in the case of the 26 December 2004 event.

Quittmeyer (1979) and Jacob and Quittmeyer (1979) used teleseismic data for earthquakes originated in MSZ to identify a shallow seismic zone that dip at about 6° (Byrne et al. 1992). It extends to about 80-km depth at the south of the volcanic arcs of the over-riding blocks (Fig. 2). The dip reaches 19° ahead of a latitude of 26.5° N and most of the earthquake activity takes place over the topmost half of the shallow dipping part of the subduction zone (Aldama-Bustos et al. 2009).

The seismicity of the Makran subduction zone is low compared with other subduction zones and exhibits strong variation between its eastern and western segments (McCall 2002). The Eastern Makran (see Fig. 2) has been ruptured several times throughout history by large events. There is some uncertainty regarding the rate of subduction in the Makran with Vernant et al. (2004) estimating a value in the range of  $19.5 \pm 2$  mm/year. GPS evidence shows significant differential movement between Oman and Iran with shortening of

**Fig. 1** The tectonic framework of the Sea of Oman is constrained by the relative motion between the Arabian, Eurasian, and Indian plates. The Eurasia subducts underneath the Arabian plate at a rate close to 2 cm/year while the relative motion between India and Arabia along the Owen strike-slip boundary reaches 3.7 mm/year



19.5 mm/year, suggesting that subduction is taking place (Masson et al. 2007).

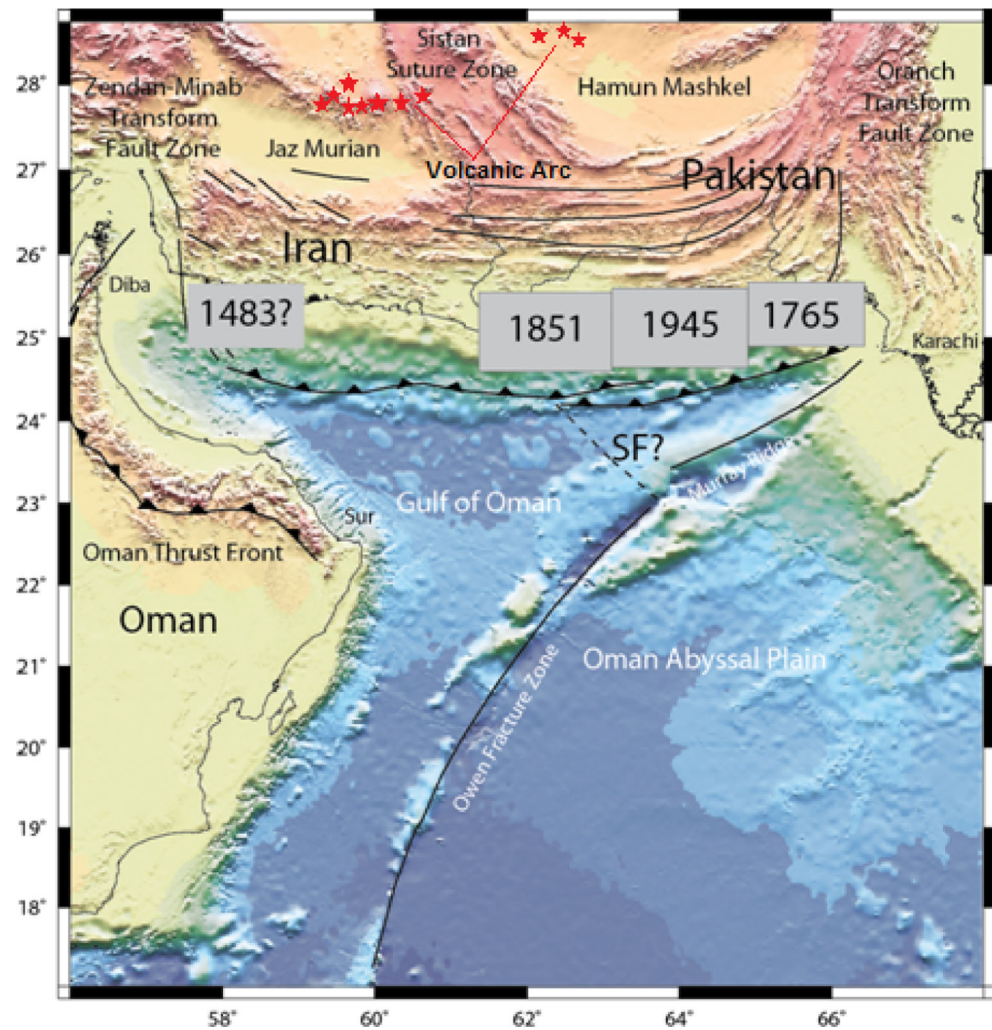
Aubin (1973) reported that an earthquake that occurred in 1483 of Ms 7.7 is responsible for the destruction of Qalhat City, Sultanate of Oman. This is the only recognized large earthquake that may strike the western part of the Makran subduction zone. It was preceded by a foreshock sequence that started in November 1482 in Hormuz. Ambraseys and Melville (1982) suggested that western Makran area is the host of this event based upon the damage of tall buildings in Hormuz in addition to the reports of Qalhat destruction at near time. On contrary, Musson (2009) concluded that Qalhat was damaged in 1497 with a local event of Mw 6.0. Lacking to reasonable basis to assume that the 1483 event was felt in Sultanate of Oman, it becomes entirely a local event to Hormuz with Mw 6.0.

The historical records place several large earthquakes in Makran since 1483. An event in 1765 was felt strongly at easternmost Makran (see Fig. 2). Two coastal events occurred in eastern Makran in 1851 and 1864, affecting the town of Gwadar (Quittmeyer 1979), while a large earthquake occurred in 1914 in northern Makran at a depth of 60–100 km, indicating that it was within the subducting plate.

On 27 November 1945, a great earthquake, of Mw 8.1, struck the coast of eastern Makran, causing about 300 deaths (Ambraseys and Melville 1982). The 1945 earthquake was an interplate thrust event that produced a slip of 6.6 m. Byrne et al. (1992) calculated the source parameters of the 1945 earthquake as seismic moment of  $1.8 \times 10^{28}$  dyn cm, moment magnitude of Mw 8.1, strike angle of  $246^\circ$ , dip angle of  $7^\circ$ , slip angle of  $89^\circ$ , and depth of  $27 \pm 3$  km. They believed that similar events would be expected to repeat at least every



**Fig. 2** Ruptured area of strong earthquakes in Makran based on Byrne et al. (1992). *SF* Sonne Fault, defining a small microplate, called the Ormara microplate, by Kukowski et al. (2000)



175 years in eastern Makran. Page et al. (1979) estimated that the recurrence of a similar 1945-type earthquake along the MSZ is approximately 125–250 years. Quittmeyer and Jacob (1979) reported the intensity (in Modified Mercalli scale), surface magnitude ( $M_s$ ), and rupture length of the 1945 event to be 10, 8, and 150–200 km, respectively. The distribution of intensities and the long-term aftershock activity suggest that the rupture propagated to the east of the epicenter (Byrne et al. 1992; Quittmeyer and Jacob 1979).

A tsunami followed the 1945 earthquake with observations along the coasts of Pakistan, Iran, and also in Oman (Mokhtari et al. 2008; Muscat Intelligence Service 1945). Several authors reported that this earthquake produced an uplift of about 2 m in some onshore coastal areas (Page et al. 1979; Ambraseys and Melville 1982).

On 16 April 2013, an earthquake with a moment magnitude of 7.7 occurred at a mountainous area in Iran, close to the border with Pakistan. The earthquake was reportedly to have occurred at an intermediate depth (80 km) within the subducting Arabian Plate below the overriding Eurasian

Plate. It was the strongest earthquake in Iran within the last 40 years and is felt as far away as the Arabian Peninsula.

On 24 September 2013, an earthquake of magnitude  $M_w = 7.7$  struck southern Pakistan. Its hypocenter, located by USGS National Earthquake Information Center was  $26.951^\circ \text{N } 65.501^\circ \text{E}$  at a depth of 15.0 km, is consistent with the rupture within the Eurasian plate above the Makran subduction zone. Less than 1 h after the earthquake, a small tsunami was recorded by the tide stations in the Oman Sea. The generated tsunami was most probably associated to submarine landslide triggered by the earthquake shaking (Heidarzadeh and Satake 2014).

### Logic-tree method for PTHA

The logic-tree is recognized as a useful method to address the probabilistic tsunami hazard assessment (Annaka et al. 2007; Burbidge et al. 2008). Here, we built a logic-tree framework

(Fig. 3) to analyze the tsunami hazard along the coast of Oman through a probabilistic approach. The developed logic-tree incorporates various nodes where each of them gives rise to a set of branches. A weight is assigned to each branch and then integrated in the probability of hazard exceedance computations. In the following sections, we present a description of each logic-tree node.

**Source zones—nodes 0 and 1 of the logic-tree**

The Makran subduction zone (MSZ, node 0 of the logic-tree, Fig. 3) is considered as the most seismogenic potential zone that might cause tsunamis that affect the northern coasts of Oman. The western part of the MSZ has not produced any known tsunamigenic earthquakes. The absence of earthquakes in this part indicates that either the western part of MSZ is entirely aseismic or that the plate boundary is presently locked. The existence of late Holocene marine terraces along both the eastern and western parts of MSZ reflects the capability of both parts to generate megathrust earthquakes.

The seismicity pattern, degree of deformation, and the rupture history are different from the eastern to the western parts of MSZ, suggesting a segmentation of the subduction zone (Minshull et al. 1992; Byrne et al. 1992). This suggestion is further supported by the offsets in the volcanic arc and by the two large-scale Paleozoic blocks dominating the overriding plate namely Lut and Helmand blocks (Byrne et al. 1992). The boundary between these two Paleozoic blocks is almost coincident with the transition and changes in seismicity between the eastern and western MSZ. Huhn et al. (1998) used swath mapping to indicate the presence of a sinistral strike-slip fault that passes through the Makran accretion. Kukowski et al. (2000) delineated this spreading center at the Murray Ridge, separating the easternmost part of the Arabian plate from the remainder by the Sonne Fault and forming the Ormara microplate, which moves separately from the remaining MSZ. This provides a reasonable interpretation of why the seismicity in the eastern part of MSZ is

significantly higher than that in the western part; simply, it is entirely separate from the western Makran (Musson 2009). These reasons prompted the authors to give the segmentation of MSZ much higher weight over being a single structure.

In this study, we consider both hypotheses that result in associating three source zones (SZ, node 1 of the logic-tree, Fig. 3) to the MSZ. They are the eastern Makran zone (EasMZ), the western Makran zone (WesMZ) (MSZ as two segments), and the entire Makran zone (EntMZ) (MSZ as one segment). On the other hand, we favor the hypothesis of the segmentation of MSZ in EasMZ and WesMZ. Therefore, we assign to the logic-tree branches (Fig. 3) a higher weight ( $W_{RM}$  in Fig. 3) of 0.85 for the segmented model versus only 0.15 weight for the entire model (Table 1).

**Scenario magnitude—node 2 of the logic-tree**

We define, within the source zone of Makran, the earthquake sources that can trigger tsunamis that may impact the coast of Oman. This set of sources constitutes the basis of the tsunamigenic scenarios for PTHA. The methodology includes the following: (i) definition of the magnitude interval for each source zone and (ii) associate a typical fault (TF) for each individual magnitude (Mg, node 2 of the logic-tree, Fig. 3).

Here, the tsunamigenic scenarios include earthquake magnitudes ranging from Mw 7.9 to 9.1 with a regular interval of 0.2 between individual magnitudes. The definition of the TF consists of establishing the dimensions of the fault (length, width, and depth) and the strike, rake, and dip angles of the earthquake mechanism. These parameters are used to compute the sea bottom deformation needed to initiate the tsunami simulation.

**Earthquake annual recurrence rates—node 3 of the logic-tree**

The historical record of earthquakes in the Makran area is too short to enable a reliable evaluation of their frequency of

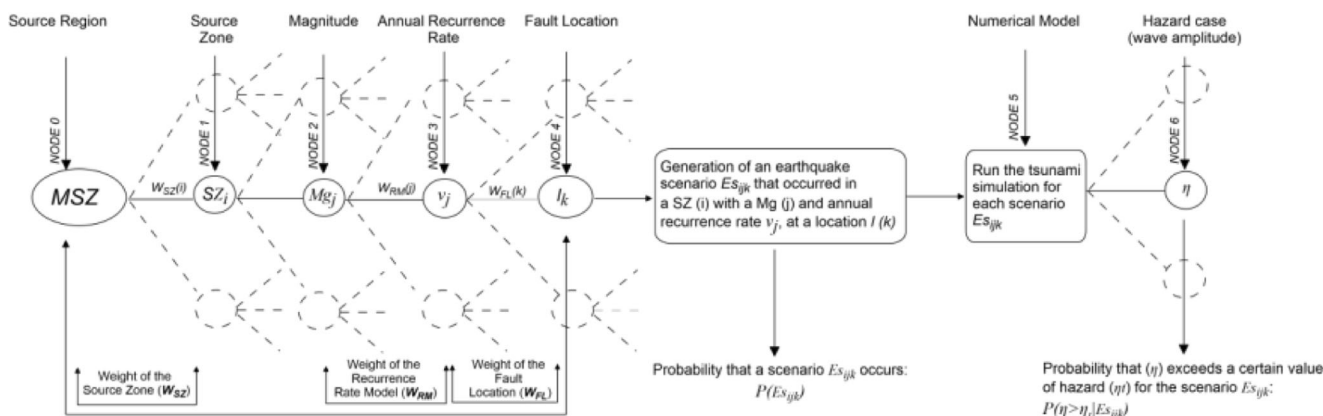


**Fig. 3** Logic tree developed for probabilistic tsunami hazard assessment along the coast of Oman

**Table 1** Weight factors used for the PTHA along the Omani coast

	Different models	Weight for each model
Source zone	Segmented model	0.85
	Entire model	0.15
Earthquake recurrence rate	Molnar (1979) model	0.4
	Deif and El-Hussain (2012) model	0.6
Fault location	Moving the TF along the fault trace	1/n, where n is the number of possible TF

occurrence; a much longer time spanning is required to evaluate the recurrence parameters correctly. Therefore, estimating the probabilistic tsunami hazard through the application of the recurrence interval of seismic history alone is neither possible nor accurate.

Since the slip rate and the earthquake occurrence are related, the rate of slip is nowadays used to constrain the parameters of occurrence-rate expressions (Anderson and Luco 1983; Tselentis et al. 1988; Yadav et al. 2010; Beghoul et al. 2010; Visini et al. 2010). Due to the linearity between the slip rate and the seismic moment rate (Brune 1968; Aki 1972; Kanamori and Anderson 1975), the latter can instead be used as a constraint on the earthquake recurrence along the active faults.

Gutenberg and Richter's (1954) law is the simplest and most widely used expression that relates the cumulative frequency of earthquake occurrence  $N(m)$  with different magnitudes ( $m$ ) (Eq. 1):

$$\log \dot{N}(m) = a - bm \quad (1)$$

where  $a$  is the seismicity rate, and  $\log N(m)$  is the logarithm of the average number of earthquakes of magnitude ( $m$ ) or larger, occurring during a specific time interval. The  $b$  value, or the negative slope of the regression straight line, indicates the relative frequency of occurrence of large and small earthquakes. Using an additional empirical relation (Eq. 2) between earthquake magnitude and the seismic moment  $M_o$

$$\log \dot{M}_o = cm + d \quad (2)$$

where  $c$  and  $d$  are the regression constants. Molnar (1979) developed a formula (Eq. 3), which relates the cumulative number of earthquake occurrence per year  $N(M_o)$  with the seismic moment ( $M_o$ ) and the rate of seismic moment release:

$$\dot{N}(M_o) = \frac{(1-\beta) \dot{M}_o M_o^{-\beta}}{M_{o\max}^{1-\beta}} \quad (3)$$

where  $M_{o\max}$  is the maximum seismic moment likely to occur in the region of interest,  $\dot{M}_o$  is the rate of seismic moment release, and  $\beta$  equals ( $b/c$ ). The  $b$  and  $c$  values are the slopes of

Eq. (1) and (2), respectively. The reciprocal of Eq. (3) is  $T(M_o)$  (the mean recurrence interval of earthquakes with specific seismic moment). Despite the relative oldness of the Molnar (1979) model, it is widely used since its release till now to determine the recurrence interval of the large earthquakes (Qin et al. 2001; Krishna and Sanu 2002; Nilgun 2005; Bus et al. 2009). The GR model is open from its both ends. This contradicts the fact of finite breaking strength of the earth's crust and the finite extent of the source zone. Therefore, the truncated Gutenberg–Richter (TGR) model is introduced to fix this disadvantage. Deif and El-Hussain (2012) modified the Molnar (1979) mathematical expression to produce a mathematical model based upon the TGR model instead of the normal Gutenberg–Richter one (Eq. 4).

$$\dot{N}(M_o) = \frac{[\dot{M}_o + \eta M_{o\max}] (1-\beta) M_o^{-\beta}}{M_{o\max}^{1-\beta}} - \eta \quad (4)$$

The parameter  $\eta$  guarantees the fact that above a certain value of maximum seismic moment, there is no earthquake. This is the main difference from the Molnar (1979) model. Herein, the recurrence interval could be expressed in terms of the rate of seismic moment release for different seismic moments. The recurrence interval of different magnitudes can also be calculated if the moment values are transformed into magnitude values using a proper empirical seismic moment–magnitude relationship.

The rate of slip along the Makran zone is measured to be 19.5 mm/year (Masson et al. 2007), suggesting that subduction is taking place. Slip rate and seismic moment release rate are related to each other by the Eq. 9:

$$\dot{M}_o = \mu A \dot{U} \quad (5)$$

where  $\dot{M}_o$  is the rate of seismic moment release,  $\mu$  is the rigidity modulus, and  $\dot{U}$  is the slip rate on the fault of area  $A$  (Brune 1968; Hanks and Kanamori 1979). Therefore, we can use the rate of slip to calculate the rate of seismic moment, which is required for the application of the developed model and to constraint the earthquake recurrence along major faults.

The rate of seismic moment release is calculated using a slip rate of 19.5 mm/year; fault width equal to 215 km; fault lengths equal to 809, 429, and 380 km for entire, east, and



west Makran, respectively; and assuming  $\mu$  to be  $3E + 11$  dyn/cm<sup>2</sup>. The seismic moment rate is found to be  $1.0436E + 27$ ,  $5.2503E + 26$ , and  $4.84E + 26$  dyn cm/year. Individual faults are assumed to have a  $b$  value equal to the regional  $b$  value. The used  $b$  value is taken to be 0.77 (Deif and El-Hussain 2012). The parameter  $\eta$  is calculated then using Eq. (4) given that the number of earthquakes with seismic moment greater than the maximum expected one is zero. The values of  $\eta$  are found to be 0.000365, 0.002795, and 0.005147 for entire, east, and west Makran, respectively. Tables 2, 3, and 4 show the recurrence intervals in EntMZ, EasMZ, and WesMZ respectively.

In this study, we consider in the probabilistic tsunami hazard calculations the outputs (earthquake recurrence intervals) from both models, namely, the Molnar (1979) model and the Deif and El-Hussain (2012) model. On the other hand, we weighted these models based on our expert opinion ( $W_{RM}$  in Fig. 3). The weight given to the Deif and El-Hussain (2012) model is slightly higher (0.6) than to the Molnar (1979) model (0.4) (see Table 1), because it better fits the compiled seismic catalog for Oman and its surrounding and also due to the consistency between the calculated recurrence interval and the observed seismological data, especially for the largest magnitudes.

#### Scenario database and tsunami simulation model—nodes 4 and 5 of the logic-tree

The generation of the scenario database consists of letting float the established  $TF$  along the fault trace, with regular intervals of half rupture length, in each  $SZ$  (Lorito et al. 2008; Heidarzadeh et al. 2008; Omira et al. 2015). Within the same fault trace and for the same magnitude scenario, the locations are considered equally probable and therefore an equal weight is attributed ( $W_{FL}$  in the logic-tree, node 4, Fig. 3). Using the fault floating process, we can generate a larger number of scenarios (see Fig. 4). Then, the tsunami numerical modeling is performed for each scenario (node 5 of the logic-tree, Fig. 3).

In this study, we used a non-linear shallow water model (NSWING) to compute the tsunami propagation from the source zone toward the coast. Nonlinear shallow water with nested grids (NSWING) (Miranda et al. 2014) is an implementation based on Liu et al. (1998), like COMCOT, entirely written in C, with an easy-to-use interface following the GMT style and core parallelism for faster computing of performance and to allow for its use in more computing-intensive problems. The code was developed to support tsunami research and applications by the Instituto Dom Luiz and the Instituto Português do Mar e da Atmosfera Tsunami Group and has been used to simulate the recent Chilean tsunami events (Omira et al. 2016b). The code uses a discretization and explicit leap-

frog finite difference scheme to solve the shallow water equations in spherical or Cartesian coordinates (Miranda et al. 2014). An open boundary condition is used on the outward limit of the grid, whenever it does not correspond to land. The code solves numerically the following set of equations:

$$\begin{aligned} \frac{\partial \eta}{\partial t} + \frac{\partial P}{\partial x} + \frac{\partial Q}{\partial y} &= -\frac{\partial h}{\partial t} \\ \frac{\partial P}{\partial t} + \frac{\partial}{\partial x} \left( \frac{P^2}{H} \right) + \frac{\partial}{\partial y} \left( \frac{PQ}{H} \right) + gH \frac{\partial \eta}{\partial x} + \tau_x H &= 0 \\ \frac{\partial Q}{\partial t} + \frac{\partial}{\partial x} \left( \frac{PQ}{H} \right) + \frac{\partial}{\partial y} \left( \frac{Q^2}{H} \right) + gH \frac{\partial \eta}{\partial y} + \tau_y H &= 0 \end{aligned} \quad (6)$$

where  $\eta$  is the free surface elevation;  $h$  is the still water depth;  $H$  is the total water depth;  $P$  and  $Q$  are the volume fluxes in  $x$  and  $y$  directions, respectively; and  $\tau_x$  and  $\tau_y$  are the bottom frictional terms.

To initiate the tsunami simulation model, we compute co-seismic deformation due to the submarine earthquake. We use the Okada (1985) equations to compute the sea bottom deformation due to the earthquake assuming that the water is an incompressible fluid; the initial sea surface elevation mimics the sea bottom deformation. The initial sea surface elevation and the zero velocity constitute the initial conditions of the simulation model.

The bathymetric grid used in this study is a compilation of multisource depth data from GEBCO (GEBCO 2014) with 30-s arc resolution and the digitized nautical maps along the generation area (Makran subduction zone). The final bathymetric dataset is a 30-arcsecond grid in geographical coordinates extending from 53.2° E to 57.8° W and from 16.2° N to 27.8° N.

We ran the tsunami simulations for 4 h of tsunami propagation to ensure that all Omani coast is reached. We use a 1-s time step, in the 30-arcsecond grid, to guarantee the CFL numerical stability condition.

#### PTHA framework—node 6 of the logic-tree

We compute the probability of exceeding specific wave amplitude threshold along the coast of Oman for given exposure times. To do this, we take into account the tsunami scenarios represented in probabilistic calculations by their recurrence rates and by the resulted wave amplitudes at the coast.

To establish, for multiple sources (scenarios  $Es_{ijk}$ , see the Fig. 3), the joint probability that a wave height exceeds a particular value for a given period, we consider that the sources are independent (as in the Poisson distribution). This process allows the calculation of the time-independent probability that wave height will be exceeded due to the occurrence of an earthquake scenario.

**Table 2** Earthquake recurrence rate for the entire Makran source zone

Moment magnitude	Seismic moment (dyne/cm <sup>2</sup> )	Annual recurrence rate (Molnar 1979)	Annual recurrence rate (Deif and El-Hussain 2012)
7.5	2.00E + 27	0.017287	0.019955
7.6	2.82E + 27	0.014478	0.016654
7.7	3.98E + 27	0.012126	0.013889
7.8	5.62E + 27	0.010156	0.011573
7.9	7.94E + 27	0.008506	0.009634
8.0	1.12E + 28	0.007124	0.008009
8.1	1.58E + 28	0.005967	0.006649
8.2	2.24E + 28	0.004997	0.005509
8.3	3.16E + 28	0.004186	0.004555
8.4	4.47E + 28	0.003506	0.003755
8.5	6.31E + 28	0.002936	0.003086
8.6	8.91E + 28	0.002459	0.002525
8.7	1.26E + 29	0.00206	0.002056
8.8	1.78E + 29	0.001725	0.001662
8.9	2.51E + 29	0.001445	0.001333
9.0	3.55E + 29	0.00121	0.001057
9.1	5.01E + 29	0.001013	0.000826

Assuming that  $ES_{ijk}$  obeys a Poisson process with the annual recurrence rate  $\nu_j$ , the annual probability that at least one event occurs is given by Eq. (7):

$$P(ES_{ijk}) = W_{SZ}(i) \times W_{FL}(k) \times (1 - \exp(-\nu_j)) \tag{7}$$

where  $W_{SZ}(i)$ , and  $W_{FL}(k)$  correspond to the weights for the source zone ( $i$ ) and the fault location ( $k$ ), respectively (Table 1).  $\nu_j$  is the annual recurrence rate calculated considering the recurrence

rates from the different models ( $\nu(j)$ ) and their weights  $W_{RM}(j)$  (Eq. (8)):

$$\nu_j = \sum_j W_{RM}(j) \times \nu(j) \tag{8}$$

As a specific example, considering an earthquake of magnitude  $M_w = 8.0$  in the EasMZ ( $W_{SZ} = 0.85$ , from Table 1) with an annual recurrence rate of  $\nu = (0.4 * 0.005932) + (0.6 * 0.008292) = 0.007348$  (calculated using Eq. (8) and

**Table 3** Earthquake recurrence rate for the east Makran source zone

Moment magnitude	Seismic moment (dyne/cm <sup>2</sup> )	Annual recurrence rate (Molnar 1979)	Annual recurrence rate (Deif and El-Hussain 2012)
7.5	2.00E + 27	0.014394	0.024107
7.6	2.82E + 27	0.012055	0.019737
7.7	3.98E + 27	0.010097	0.016076
7.8	5.62E + 27	0.008457	0.01301
7.9	7.94E + 27	0.007083	0.010442
8.0	1.12E + 28	0.005932	0.008292
8.1	1.58E + 28	0.004968	0.006491
8.2	2.24E + 28	0.004161	0.004982
8.3	3.16E + 28	0.003485	0.003719
8.4	4.47E + 28	0.002919	0.00266
8.5	6.31E + 28	0.002445	0.001774
8.6	8.91E + 28	0.002048	0.001032
8.7	1.26E + 29	0.001715	0.00041
8.8	1.78E + 29	0.001436	0



**Table 4** Earthquake recurrence rate for the west Makran source zone

Moment magnitude	Seismic moment (dyne/cm <sup>2</sup> )	Annual recurrence rate (Molnar 1979)	Annual recurrence rate (Deif and El-Hussain 2012)
7.5	2.00E + 27	0.018573	0.032619
7.6	2.82E + 27	0.015556	0.026484
7.7	3.98E + 27	0.013029	0.021345
7.8	5.62E + 27	0.010912	0.017041
7.9	7.94E + 27	0.009139	0.013436
8.0	1.12E + 28	0.007654	0.010417
8.1	1.58E + 28	0.006411	0.007889
8.2	2.24E + 28	0.005369	0.005771
8.3	3.16E + 28	0.004497	0.003997
8.4	4.47E + 28	0.003766	0.002511
8.5	6.31E + 28	0.003155	0.001267
8.6	8.91E + 28	0.002642	0.000225
8.7	1.26E + 29	0.002213	0

recurrence values from Table 3), the annual probability that it occurs somewhere in the EasMZ (using Eq. (7)) is  $P_1 = 0.85 * (1 - \exp(-0.007384)) = 0.00625$ .

And its annual probability of occurrence at a specific location (including the fault location weight of  $W_{FL} = 1/5$  in the

case of  $M_w = 8.0$ ) along the EasMZ is  $P_2 = 0.2 * 0.00625 = 0.00125$ .

Considering a total of  $J$  possible scenarios, the probability that the amplitude of a tsunami wave ( $\eta$ ) exceeds a threshold level ( $\eta_t$ ) during a time period ( $T$ ) is calculated as follows (Eq. (9)):

$$P(\eta > \eta_t) = 1 - \prod_{j=1}^J \left[ 1 - (1 - \exp(-\nu_j T)) \sum_{i,j,k} (W_{SZ}(i) \times W_{FL}(k)) P(\eta > \eta_t | Es_{ijk}) \right] \tag{9}$$

where  $P(\eta > \eta_t | Es_{ijk})$  is the probability that the tsunami wave associated to the  $Es_{ijk}$  scenario (computed using the tsunami numerical modeling) exceeds ( $\eta_t$ ). This probability is expressed by Eq. (10):

$$P(\eta > \eta_t | Es_{ijk}) = \begin{cases} 1 & \text{if } \eta > \eta_t \\ 0 & \text{if not} \end{cases} \tag{10}$$

**Results and discussion**

Results presented here concern only the tsunamis generated by earthquakes in the Makran subduction zone. We show maps of probabilistic tsunami exceedance for four different exposure times of 100, 250, 500, and 1000 years.

**Fig. 4** The approach for multiple tsunami scenarios' generation; the case of the entire Makran source zone

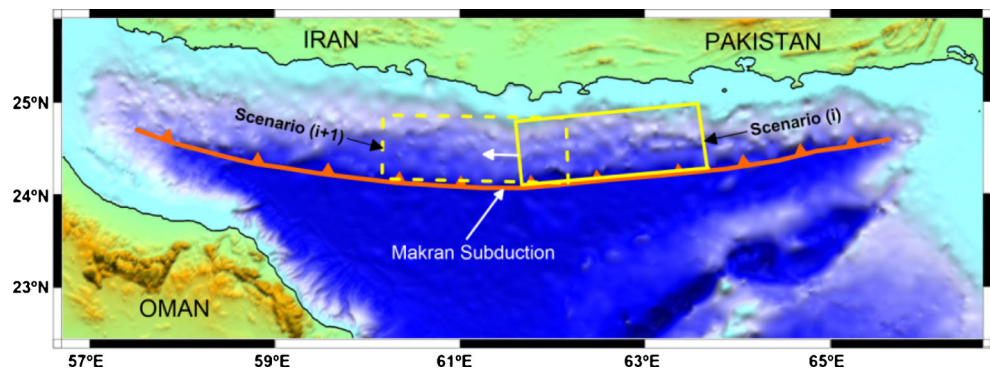
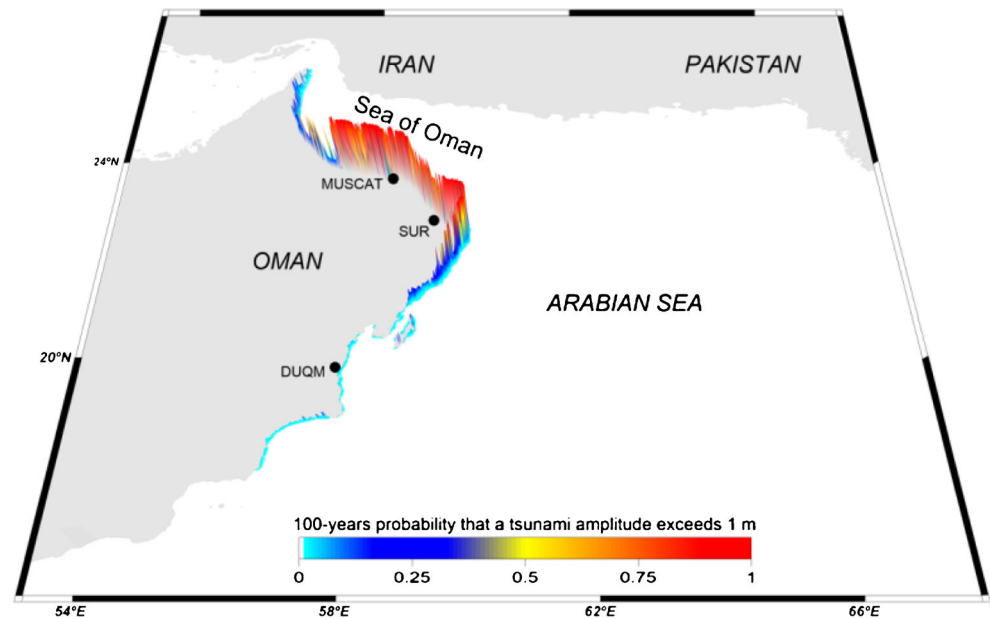


**Fig. 5** One hundred-year probability that a tsunami wave amplitude would exceed 1 m along the coast of Oman



### One hundred-year exposure time probability

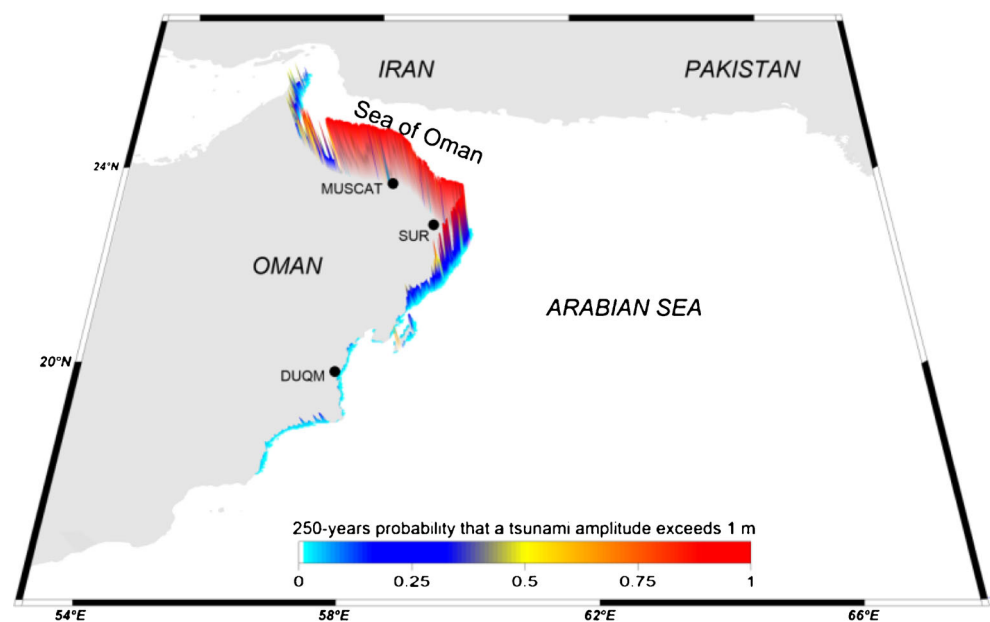
Figure 5 depicts the probability of a tsunami exceeding the 1 m wave amplitude in 100 years of exposure time. Results presented in Fig. 5 take in consideration the weights assigned to the source zones, to the fault location, and to the used earthquake recurrence models by Molnar (1979) and Deif and El-Hussain (2012). For the area between Sur and Muscat, the probability that a tsunami wave exceeds 1 m in amplitude is relatively high with values ranging from 0.5 to 0.7 (Fig. 5).

These values decrease significantly to less than 0.2 toward the western limit of the Sea of Oman and less than 0.1 toward the southern coast, close to Duqm. The coast south of Duqm remains a less hazardous Omani coastal zone from the tsunamis generated in the Makran subduction zone.

### Two hundred fifty-year exposure time probability

In Fig. 6, we present the results of probabilistic tsunami hazard assessment along the Omani coast for 250 years

**Fig. 6** Two hundred fifty-year probability that a tsunami wave amplitude would exceed 1 m along the coast of Oman



of exposure time. The map depicts the probability that a tsunami wave exceeds 1 m in amplitude considering the logic-tree framework developed for the PTHA in the region. The analysis of these results clearly shows that the northern coast of Oman, from Sur to the western limit of the Sea of Oman, is highly threatened by tsunamis generated along the Makran subduction zone. The probability of exceeding the 1 m tsunami wave ranges from 0.4 to 0.85 along this coastal segment, being at maximum close to Muscat. To the south, the probability values are noticeably low. This is due to the fact that the tsunamis triggered along the Makran subduction zone reach the southern coast, particularly south of Duqm, with wave amplitudes less than 1 m.

**Five hundred-year exposure time probability**

In Fig. 7, we plot the distribution, along the Omani coast, of the estimated probability of exceeding the threshold of the 1 m wave amplitude in 500 years of exposure time. As for the previous exposure times, the logic-tree framework described in the methodology was considered for the 500-year probability calculations. The analysis of these results shows that the 500-year probability of exceeding the 1 m tsunami amplitude reaches about 1 along the northern coast of Oman. The coastal segment between Sur and Muscat is the most tsunami hazardous zone of Oman. Similar to the results obtained for the 100 and 250 years of exposure times, the probability along the southern coasts becomes lower due to the location of these areas relative to the tsunamigenic

sources in the Makran subduction zone. At the Duqm coastal zone, the probability is close to 0.1.

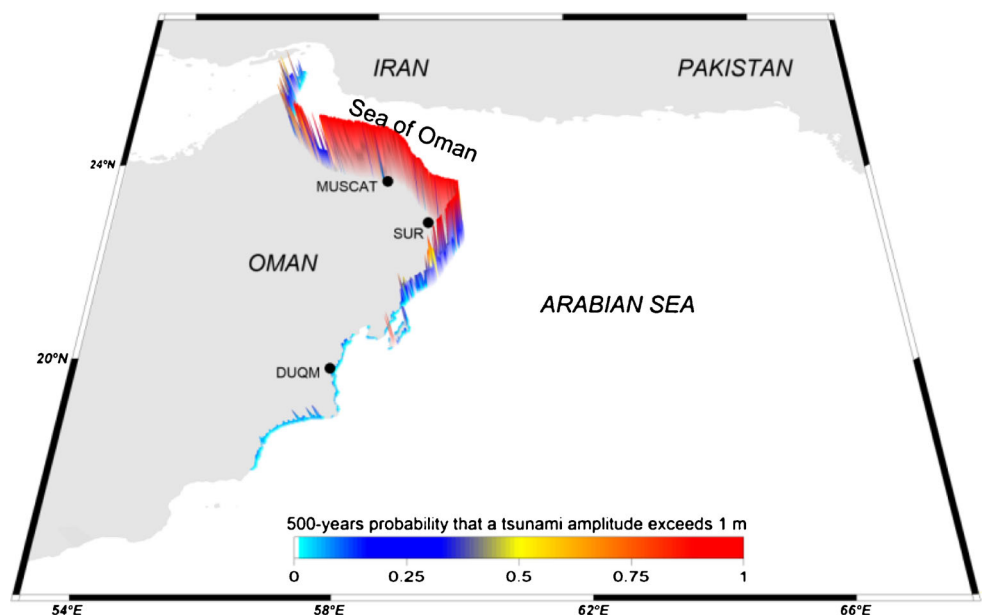
**One thousand-year exposure time probability**

Figure 8 depicts the tsunami probability results along the coast of Oman for 1000 years of exposure time. As expected, the probability to exceed the 1 m tsunami amplitude along the Omani coast increases with the increase of the exposure time. The 1000-year map shows that the probability of exceeding the 1 m tsunami is 1 along the northern coast of Oman from Sur to Muscat. It reaches also 0.8 toward the western limit of the Sea of Oman. To the south, the tsunami probabilistic map (Fig. 8) shows values close to 0.2 in the Duqm and surrounding coast.

In summary, the derived probabilistic tsunami hazard maps, considering the different exposure times of 100, 250, 500, and 1000 years, show that the northern coast facing the Sea of Oman is the most hazardous zone from tsunamis generated along the Makran subduction zone. This is mainly due to the fact that most tsunami energy associated to Makran earthquakes is steered toward the coastal segment between Sur and Muscat, particularly for the scenarios located within the western Makran source zone. The obtained results would change if additional source zones such as the Owen Ridge in the Arabian Sea and the far-field Andaman Sumatra subduction zone in the Indian Ocean are considered. These source zones should be taken into account in future works to complete the present study on PTHA.

Moreover, the attributed weights for both the source zones and the earthquake recurrence rate models control the tsunami

**Fig. 7** Five hundred-year probability that a tsunami wave amplitude would exceeds 1 m along the coast of Oman



probability estimates along the coasts of Oman. In general, the weights in PTHA are defined on the basis of expert opinion that can change from an expert to another, leading to changes in the PTHA results.

Our results agree well with previous studies from Heidarzadeh and Kijko (2011) and Hoechner et al. (2016) showing that the most hazardous area in Oman is the northeast coast, in particular, the segment between Muscat and Sur. The results obtained here also agree well with those presented by Heidarzadeh and Kijko (2011) and Hoechner et al. (2016) for the probability of a tsunami exceeding 1 m in spite of the different methodologies used to define the tsunami sources and their recurrence. For the 500-year exposure time, Hoechner et al. (2016) also present about 100 % probability of exceeding the 1 m tsunami amplitude.

## Conclusions

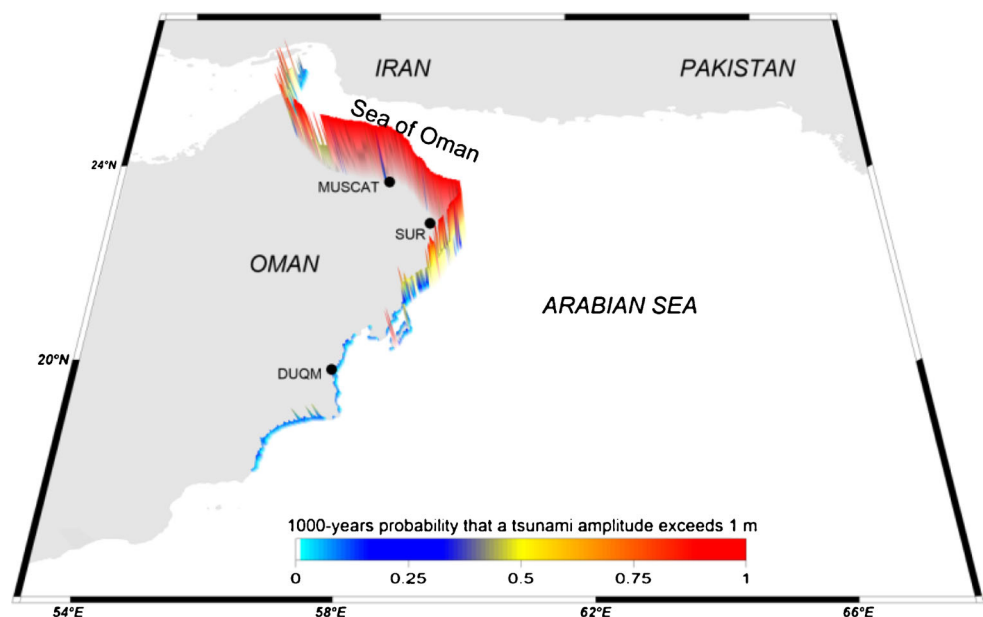
This study constitutes the first probabilistic estimate of tsunami hazard along the entire coast of Oman using a logic-tree approach. The results are expressed in terms of exceedance maps. They show that the entire coast may be affected by tsunami events of seismic origin generated along the Makran subduction zone. The study is restricted to near-field tsunami sources and includes earthquake-induced tsunamis only. Although, we recognize that the far-field sources and landslide-induced tsunamis may be important for complete tsunami hazard assessment in this area. We present the probability exceedance maps that express the likelihood that a maximum wave amplitude exceeds the 1 m threshold along

the Omani coast for four selected exposure times of 100, 250, 500, and 1000 years. The main findings of this study are as follows:

1. The probability that a maximum wave amplitude would exceed 1 m in some coastal locations of Oman reaches 0.7 and 0.85 for the 100- and 250-year exposure times, respectively.
2. Considering the exposure, larger exposure times of 500 and 1000 years, the probability that a maximum wave amplitude would exceed 1 m reaches 100 % at some locations along the northern Omani coast.
3. The northern coast of Oman is the most tsunami hazardous zone. For the four selected exposure times, higher exceedance probability values are estimated for the northern coast of Oman that includes Sur and Muscat and localities facing the Sea of Oman.
4. To the south, the tsunami hazard is less significant as most considered tsunamis, from scenarios along the Makran subduction zone, reach the southern coast of Oman with wave amplitudes less than 1 m.

It is important to mention here that there are uncertainties inherent to the results presented, namely, the weighting of the source zones, the estimation of the annual recurrence of earthquakes, the tsunami numerical model, and the bathymetric data. Also, this study suffers from the limitation of considering near-field tsunami sources of seismic origin only. Despite these limitations, the study presents an important contribution to the assessment of tsunami hazard along the coast of Oman. The results presented here may be used as a reference and input for local studies.

**Fig. 8** One thousand-year probability that a tsunami wave amplitude would exceed 1 m along the coast of Oman





**Acknowledgments** This work was done in the framework of the project on Tsunami Hazard Assessment for the Oman Liquefied Natural Gas. We would like to express our appreciation to the Oman Liquefied Natural Gas (OLNG) for funding this project. Our sincere thanks are due to the OLNG staff: Hamed Al-Naamani, Nasser Al-Makhroumi, Salim Al-Harrassy, and Najim Al-Araimi for their support. We would like also to thank all the staff of the Earthquake Monitoring Center of Sultan Qaboos University for their continuous interest and their assistance in the completion of this work. The authors wish to thank the reviewers of the paper for their comments and corrections that greatly improved the paper.

## References

- Aki K (1972) Earthquake mechanism. *Tectonophysics* 13:423–446
- Aldama-Bustos G, Bommer JJ, Fenton CH, Stafford PJ (2009) Probabilistic seismic hazard analysis for rock sites in the cities of Abu Dhabi, Dubai and Ra's Al Khymah, United Arab Emirates. *Georisk* 3-1:1–29. doi:10.1080/17499510802331363
- Allen SCR, Greenslade DJM (2010) Model-based tsunami warnings derived from observed impacts. *Nat Hazards Earth Syst Sci* 10: 2631–2642
- Ambraseys NN, Melville CP (1982) A history of Persian earthquakes. Cambridge Univ. Press, Cambridge
- Anderson JG, Luco JE (1983) Consequences of slip rate constraints on earthquake occurrence relations. *Bull Seismol Soc Am* 73(2):471–496
- Annaka T, Satake K, Sakakiyama T, Yanagisawa K, Shuto N (2007) Logic-tree approach for probabilistic tsunami hazard analysis and its applications to the Japanese coasts. *Pure Appl Geophys* 164:577–592
- Aubin J (1973) Le Royaume d'Ormuz au de'but du XVIe Sie'cle. *Mare Luso-Indicum* 4:77–179
- Beghoul N, Chatelian J, Boughach M, Benhallou H, Dadou R, Slach A (2010) Seismic empirical relations for the Tellian atlas, North Africa, and their usefulness for seismic risk assessment. *Pure Appl Geophys* 167:277–321
- Berberian M, King GCP (1981) Towards a paleogeography and tectonic evolution of Iran. *Can J Earth Sci* 18-2:210–265. doi:10.1139/e81-019
- Brune JN (1968) Seismic moment, seismicity and rate of slip along major faults zones. *Journal Geophysical Research* 73:777–784
- Burbidge D, Cummins PR, Mleczko R, Thio HK (2008) A probabilistic tsunami hazard assessment for Western Australia. *Pure Appl Geophys* 165(11–12):2059–2088
- Burbidge DR, Cummins PR, Mleczko R, Latief H, Mokhtari M (2009). A probabilistic tsunami hazard assessment of the Indian Ocean nations. s.l. : Geoscience Australia Professional Opinion No. 2009/11. <https://d28rz98at9flks.cloudfront.net/68717/68717.pdf>. Assessed 2 May 2016
- Bus Z, Gerenczy G, Toth L, Monus P (2009) Active crustal deformation in two seismogenic zones of the Pannonian region—GPS versus seismological observations. *Tectonophysics* 474:343–352. doi:10.1016/j.tecto.2009.02.045
- Byrne DE, Sykes LR, Davis SM (1992) Great thrust earthquakes and aseismic slip along the plate boundary of the Makran subduction zone. *J Geophys Res* 97(B1):449–478. doi:10.1029/91JB02165
- Coppersmith KJ, Youngs RR (1986). Capturing uncertainty in probabilistic seismic hazard assessments within intraplate tectonic environments. *Proceedings of the Third U.S. National Conference on Earthquake Engineering*, Charleston, South Carolina, pp. 301–312
- Deif A, El-Hussain I (2012) Seismic moment rate and earthquake mean recurrence interval in the major tectonic boundaries around Oman. *J Geophys Eng* 9:773–783. doi:10.1088/1742-2132/9/6/773
- DeMets D, Gordon RG, Argus DF (2010) Geologically current plate motions. *Geophys J Int* 181:1–80. doi:10.1111/j.1365-246X.2010.04491.x
- Edwards RA, Minshull TA, White RS (2000) Extension across the Indian-Arabian plate boundary: the Murray ridge. *Geophys J Int* 142(2):461–477. doi:10.1046/j.1365-246x.2000.00163.x
- Fournier M, Chamot-Rooke N, Rodriguez M, Huchon P, Petit C, Beslier M-O, Zaragosi S (2011) Owen fracture zone: the Arabia-India plate boundary unveiled. *Earth Planet Sci Lett* 302:247–252. doi:10.1016/j.epsl.2010.12.027
- GEBCO (2014). The general bathymetric chart of the oceans, GEBCO\_2014 Grid, version 20150318, available at: <http://www.gebco.net>, last access: September
- Geist EL, Lynett PJ (2014) Source processes for the probabilistic assessment of tsunami hazards. *Oceanography* 27(2):86–93
- Geist EL, Parsons T (2006) Probabilistic analysis of tsunami hazards. *Nat Hazards* 37(3):277–314. doi:10.1007/s11069-005-4646-z
- González FI, Geist EL, Jaffé B, Kânoğlu U, Mofjeld H, Synolakis CE, Titov VV, Arcas D, Bellomo D, Carlton D, Horning T (2009) Probabilistic tsunami hazard assessment at seaside, Oregon, for near- and far-field seismic sources. *J Geophys Research (Oceans)* 114(C11):1978–2012
- Gutenberg B, Richter CF (1954) Seismicity of the earth and associated phenomena. S.L. Hafner, New York
- Hanks TC, Kanamori K (1979) A moment magnitude scale. *J Geophys Res* 84(B5):2348–2350. doi:10.1029/JB084iB05p023489B0059
- Harms JC, Cappel HN, Francis DC (1984) The Makran coast of Pakistan: its stratigraphy and hydrocarbon potential. Marine geology and oceanography of Arabian Sea and coastal Pakistan. Van Nostrand Reinhold, New York, pp. 3–26
- Heidarzadeh M, Kijko A (2011) A probabilistic tsunami hazard assessment for the Makran subduction zone at the northwestern Indian Ocean. *Nat Hazards* 56(3):577–593. doi:10.1007/s11069-010-9574-x
- Heidarzadeh M, Satake K (2014) Possible sources of the tsunami observed in the northwestern Indian Ocean following the 2013 September 24 Mw 7.7 Pakistan inland earthquake. *Geophys J Int* 199(2):752–766
- Heidarzadeh M, Pirooz MD, Zaker NH, Yalciner AC, Mokhtari M, Esmaily A (2007) Historical tsunamis in the Makran subduction zone off the southern coasts of Iran and Pakistan and results of numerical modeling. *Ocean Eng* 30-35(8):774–786. doi:10.1016/j.oceaneng.2008.01.017
- Heidarzadeh M, Pirooz MD, Zaker NH, Synolakis CE (2008) Evaluating tsunami hazard in the northwestern Indian Ocean. *Pure Appl Geophys* 165(11–12):2045–2058
- Hoechner A, Babeyko AY, Zamora N (2016) Probabilistic tsunami hazard assessment for the Makran region with focus on maximum magnitude assumption. *Nat Hazards Earth Syst Sci* 16:1339–1350. doi:10.5194/nhess-16-1339-2016
- Huhn K, Kukowski N, Schillhorn T, Flueh E (1998) Morphotectonics of the Makran accretionary wedge imply new aspects for the plate tectonic situation in the northeast Indian Ocean. [http://www.geomar.de/add\\_info/former\\_info/abstracts98/agu98abstracts.html](http://www.geomar.de/add_info/former_info/abstracts98/agu98abstracts.html) Accessed 23-25 May 2006
- Jacob KH, Quittmeyer RL (1979) The Makran region of Pakistan and Iran: trench-arc system with active plate subduction. *Geodynamics of Pakistan: 305–317*. eds Farah, A. de Jong, K.A., Geological Survey of Pakistan, Quetta
- Kanamori H, Anderson DL (1975) Theoretical basis of some empirical relations in seismology. *Bull Seismol Soc Am* 65(5):1073–1095
- Kopp C, Fruehn J, Flueh ER, Reichert C, Kukowski N, Bialas J, Klaeschen D (2000) Structure of the Makran subduction zone from wide angle and reflection seismic data. *Tectonophysics* 329:171–191. doi:10.1016/S0040-1951(00)00195-5

- Krishna R, Sanu T (2002) Shallow seismicity, stress distribution and crustal deformation patterns in the Andaman-west Sunda arc and Andaman Sea, northeastern Indian Ocean. *J Seismol* 6:25–41
- Kukowski N, Schillhorn T, Flueh ER, Huhn K (2000) Newly identified strike-slip plate boundary in the northeastern Arabian Sea. *Geology* 28(4):355–358. doi:10.1130/0091-7613
- Liu PLF, Woo SB, Cho YS (1998). Computer programs for tsunami propagation and inundation. Technical report, Cornell University
- Lorito S, Tiberti MM, Basili R, Piatanesi A, Valensise G (2008) Earthquake-generated tsunamis in the Mediterranean Sea: scenarios of potential threats to southern Italy. *J Geophys Res Solid Earth* 113(B1):1978–2012
- Lorito S, Selva J, Basili R, Romano F, Tiberti MM, Piatanesi A (2015) Probabilistic hazard for seismically induced tsunamis: accuracy and feasibility of inundation maps. *Geophys J Int* 200(1):574–588
- Masson F, Anvari M, Djamour Y, Walpersdorf A, Tavakoli F, Daignieres M, Nankali H, Van Gorp S (2007) Large-scale velocity field and strain tensor in Iran inferred from GPS measurements: new insight for the present-day deformation pattern within NE Iran. *Geophys J Int* 170:436–440. doi:10.1111/j.1365-246X.2007.03477.x
- McCall GJH (2002) A summary of the geology of the Iranian Makran. In: Clift PD, Kroon D, Gaedicke C, Craig J (eds) *The tectonic and climatic evolution of the Arabian Sea region*, vol 195. Geological Society, London Special Publications, pp. 147–204
- Minshull TA, White RS, Barton PJ, Collier JS (1992) Deformation at plate boundaries around the Gulf of Oman. *Mar Geol* 104:265–277
- Miranda JM, Luis J, Reis C, Omira R, Baptista MA (2014). Validation of NSWING, a multicore finite difference code for tsunami propagation and run up. American Geophysical Union Fall Meeting, S21 A4390. <http://adsabs.harvard.edu/abs/2014AGUFM.S21A4390M>
- Mokhtari M, Fard IA, Hessami K (2008) Structural elements of the Makran region, Oman Sea and their potential relevance to tsunamigenesis. *Nat Hazards* 47(2):185–199. doi:10.1007/s11069-007-9208-0
- Molnar P (1979) Earthquake recurrence intervals and plate tectonics. *Bull Seismol Soc Am* 69:115–133
- Muscat Intelligence Summary (1945). Public Record Office Document. United Kingdom : India Office Records IOR R/15/6/359. British Library
- Musson RMW (2009) Subduction in the western Makran: the historian's contribution. *J Geol Soc* 166(3):387–391. doi:10.1144/0016-76492008-119
- Nagarajan B, Suresh I, Sundar D, Sharma R, Lal AK, Neetu S, Shenois SS, Shetye SR, Shankar D (2006) The great tsunami of 26 December 2004: a description based on tide-gauge data from the Indian sub-continent and surrounding areas. *Earth Planets Space* 58(2):211–215. doi:10.1186/BF03353380
- Nilgun S (2005) An application of the time and magnitude-predictable model to long-term earthquake prediction in eastern Anatolia. *J Seismol* 9:367–379
- Okada Y (1985) Surface deformation due to shear and tensile faults in a half-space. *Bull Seismol Soc Am* 75.4(1985):1135–1154
- Okal E, Fritz HM, Synolakis CE, Raad PE, Al-Shijbi Y, Al-Saifi M (2006) Field survey of the 2004 Indonesian tsunami in Oman. *Earthquake Spectra* 22:S203–S218. doi:10.1193/1.2202647
- Omira R, Baptista MA, Matias LM (2015) Probabilistic tsunami hazard in the Northeast Atlantic from near and far-field tectonic sources. *Pure Appl Geophys* 172(3–4):901–920. doi:10.1007/s00024-014-0949-x
- Omira R, Matias LM, Baptista MA (2016a) Developing an event-tree probabilistic tsunami inundation model for NE Atlantic coasts: application to a case study. *Pure Appl Geophys*. doi:10.1007/s00024-016-1367-z
- Omira R, Baptista MA, Lisboa F (2016b) Tsunami characteristics along the Peru–Chile trench: analysis of the 2015 Mw8.3 Illapel, the 2014 Mw8.2 Iquique and the 2010 Mw8.8 Maule tsunamis in the near-field. *Pure Appl Geophys* 173:1063–1077
- Page WD, Alt JN, Cluff LS, Plafker G (1979) Evidence for the recurrence of large-magnitude earthquakes along the Makran coast of Iran and Pakistan. *Tectonophysics* 52(1):533–547. doi:10.1016/0040-1951(79)90269-5
- Pendsee CG (1946) The Mekran earthquake of the 28th November 1945. *India Meteorol depart Sci. Notes* 10(125):141–145
- Power W, Downes G, Stirling M (2007) Estimation of tsunami hazard in New Zealand due to south American earthquakes. *Pure Appl Geophys* 164:547–564
- Qin C, Papadimitriou EE, Papazachos BC, Karakaisis GF (2001) Time-dependent seismicity in China. *J Asian Earth Sc* 19(1):97–128. doi:10.1016/S1367-9120(00)00019-5
- Quittmeyer RC (1979) Seismicity variations in the Makran region of Pakistan and Iran: relation to great earthquake. *Pure Appl Geophys* 117:1213–1228. doi:10.1007/BF00876216
- Quittmeyer RC, Jacob KH (1979) Historical and modern seismicity of Pakistan, Afghanistan, northwestern India, and southeastern Iran. *Bull Seismol Soc Am* 69:773–823
- Rabinovich AB, Thomson RE (2007) The 26 December 2004 Sumatra tsunami: analysis of tide gauge data from the world ocean part 1. Indian Ocean and South Africa. In *Tsunami and Its Hazards in the Indian and Pacific Ocean*: 261–308. doi:10.1007/s00024-006-0164-5
- Rikitake T, Aida I (1988) Tsunami hazard probability in Japan. *Bull Seismol Soc Am* 78(3):1268–1278
- Rodriguez M, Chamot-Rooke N, Hébert H, Fournier M, Huchon P (2013) Owen ridge deep-water submarine landslides: implications for tsunami hazard along the Oman coast. *Nat Hazards Earth Syst Sci* 13:417–424
- Roshan AD, Basu PC, Jangid RS (2016) Tsunami hazard assessment of Indian coast. *Nat Hazards* 82:733–762. doi:10.1007/s11069-016-2216-1
- Sørensen MB, Spada M, Babeyko A, Wiemer S, Grünthal G (2012) Probabilistic tsunami hazard in the Mediterranean Sea. *Journal of Geophysical Research (Solid Earth)* 117(B1):1978–2012
- Swapna M, Srivastava K (2014) Effect of Murray ridge on the tsunami propagation from Makran subduction zone. *Geophys J Int* 199(3):1430–1441
- Tselentis GA, Stavrakakis G, Makropoulos K, Latousakis J, Drakopoulos J (1988) Seismic moments of earthquakes at the western Hellenic arc and their application to the seismic hazard of the area. *Tectonophysics* 148:73–82
- Vernant P, Nilforoushan F, Hatzfeld D, Abassi MR, Vigny C, Masson F, Nankali H, Martinod J, Ashtiani A, Bayer R, Tavakoli F, Chery J (2004) Present-day crustal deformation and plate kinematics in Middle East constrained by GPS measurements in Iran and northern Oman. *Geophys J Int* 157:381–398. doi:10.1111/j.1365-246X.2004.02222.x
- Visini F, Nardis R, Lavecchia A (2010) Rates of active compressional deformation in Central Italy and Sicily, evaluation of the seismic budget. *International Journal of Earth Science* 99:S243–S264
- Wiens DA, DeMets C, Gordon RG, Stein S, Argus D, Engeln JF, Lundgren P, Quible D, Stein C, Weinstein S, Woods DF (1985) A diffuse plate boundary model for Indian Ocean tectonics. *Geophys Res Lett* 12(7):429–432
- Yadav RBS, Shanker D, Chopra S, Singh A (2010) An application of regional time and magnitude predictable model for long-term earthquake prediction in the vicinity of October 8, 2005 Kashmir Himalaya earthquake. *Natural Hazard* 54:985–1014
- Yadav RBS, Tripathi JN, Kumar TS (2013) Probabilistic assessment of tsunami recurrence in the Indian Ocean. *Pure Appl Geophys* 170(3): 373–389. doi:10.1007/s00024-012-0487-3